ISSN 0023-1584, Kinetics and Catalysis, 2008, Vol. 49, No. 2, pp. 279–284. © MAIK "Nauka/Interperiodica" (Russia), 2008.
Published in Russian in Kinetika i Kataliz, 2008, Vol. 49, No. 2, pp. 293–299.

Photocatalytic Degradation of Organic Compounds in Aqueous Systems by Fe and Ho Codoped TiO_2[1]

J. Shi, J. Zheng, Y. Hu, and Yu. Zhao

The State Key Laboratory of Heavy Oil, China University of Petroleum, Dongying, Shandong, 257061 P. R. China
e-mail: shijnwn@163.com

Received January 20, 2007

Abstract—Undoped, single-doped, and codoped TiO_2 nanoparticles were prepared by the sol-gel method and characterized with X-ray diffraction (XRD), the Brunauer-Emmett-Teller (BET)-specific surface area (S_{BET}), UV-Vis absorption spectra (UV-Vis), and X-ray photoelectron spectroscopy (XPS). Their photocatalytic activity was evaluated by methyl orange (MO) degradation in an aqueous suspension under UV or simulated solar light illumination. XRD showed that all samples calcined at 600°C preserved the anatase structure, and doping inhibited the increase of crystallite size. The BET result revealed that doping improved the surface area of TiO_2. UV-Vis indicated that Fe^{3+}-doping broadened the absorption profile of TiO_2. XPS demonstrated that doping was advantageous to absorb more surface hydroxyl groups or chemisorbed water molecules. Photocatalytic degradation showed that the photocatalytic activity of TiO_2 codoped with Fe^{3+} and Ho^{3+} ions was markedly improved. This was ascribed to the fact that there was a cooperative action in the two doped elements. Fe^{3+}-doping broadens the absorption profile, improves photo utilization of TiO_2, and then generates more electron-hole pairs. Ho^{3+}-doping restrains the increase in grain size and retards the recombination of photo-generated electrons and holes.

DOI: 10.1134/S002315840802016X

1. INTRODUCTION

Colored wastewater is released in textile effluents and poses a potential environmental hazard. Within the ecosystem, this colored wastewater is a dramatic source of pollution, eutrophication, and perturbations in aquatic life. Moreover, a variety of organic chemicals are produced during the dyeing process, and some have been shown to be carcinogenic [1]. With the growing awareness of decreasing available water resources, many methods, including physical, chemical, and biological methods, are being used in wastewater treatment and recycling. Among them, heterogeneous photocatalysis appears to be an emerging destructive technology leading to the total mineralization of most organic pollutants [2–7], in which TiO_2 is widely used because of its optical and electronic properties, low cost, chemical stability, and nontoxicity [8]. However, TiO_2 utilizes only a very small fraction of the solar spectrum due to its band-gap energy, and the photocatalytic activity of TiO_2 is limited by fast charge-carrier recombination and low interfacial charge-transfer rates of photogenerated carriers. In order to improve its photocatalytic activity, many studies have been undertaken. The results show that selective metal ion doping is one of the effective means. In the present study, the investigations about doping elements focus primarily on doping of transition metal ions [9–14]. Rare earth metals that have incompletely occupied the 4*f* and empty 5*d* orbitals often serve as a catalyst or promote catalysis. Some results show that the photocatalytic activity of TiO_2 can be improved because of the doping of some rare earth metals [15–18].

Codoping with two kinds of ions has been investigated in recent years and has received attention from many investigators [19–21]. Wang et al. [22] found that, under the irradiation of light with wavelengths larger than 400 and 290 nm, the photocatalytic activity of nitrogen and lanthanum codoped $SrTiO_3$ was 2.6 and two times greater than that of pure $SrTiO_3$. Zhang et al. [23] found that Pt deposited onto Nb^{5+}/TiO_2 increased the photodegradation activity of $CHCl_3$. These facts indicate that introducing two or more proper elements onto nanocrystalline TiO_2 particles will improve the photocatalytic effect of TiO_2. Codoping transition metal ions and rare earth metal onto nanocrystalline TiO_2 may have a synergistic effect to increase the activity of TiO_2.

In this work, TiO_2 codoped with Fe^{3+} and Ho^{3+} was prepared by the sol-gel method and a systematic characterization was conducted. The photocatalytic activity was evaluated by photodegradation of methyl orange in solution under UV light and simulated solar light irradiation. We found that the codoping with Fe^{3+} and Ho^{3+} could obviously enhance the photocatalytic activity for the methyl orange degradation relative to undoping and single-doping TiO_2. A relationship between the structure and the photoactivity of samples was proposed, and the synergistic effect of two dopants leading to sig-

[1] This article was submitted by the authors in English.

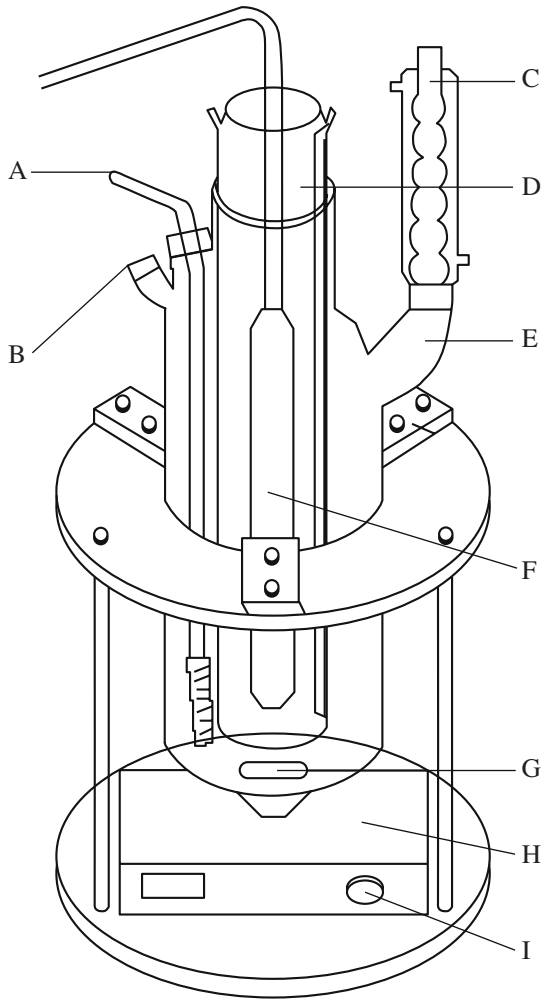

Fig. 1. Schematic figure of the photo reaction system: (A) Temperature probe; (B) Blowhole; (C) Condensator; (D) Water-cooled quartz jacket; (E) Reactive bottle; (F) Lamp; (G) Magnetic rod; (H) Magnetic stirrer; (I) Velocity knob.

nificant enhancement of photodegradation has been discussed.

2. EXPERIMENTAL

2.1. Synthesis of Doped TiO_2 Photocatalysts

TiO_2 nanoparticles codoped with Fe^{3+} and Ho^{3+} were prepared by the sol-gel route using tetra-n-butyl titanate, transition metal salts $Fe(NO_3)_3 \cdot 9H_2O$, and the rare earth metal salts $Ho(NO_3)_3 \cdot 6H_2O$ as the precursors. In the molar ratio $Ti(OC_4H_9)_4 : C_2H_5OH : H_2O : CH_3COOH = 1 : 8 : 20 : 6$, 0.05 mol $Ti(OC_4H_9)_4$ (C.P.) was dissolved in 30 mL ethanol with stirring for 30 min. Another solution containing 28.32 mL ethanol, 7.2 mL H_2O, 20 mL acetic acid, transition metal salts, and rare earth metal salts in the required stoichiometry was slowly added into the above solution under magnetic stirring at room temperature. The mixture was hydrolyzed for 60 min under vigorous stirring, and a transparent sol was obtained. The gel was prepared by aging the sol for 6 h at 60°C. The derived gel was dried at 80°C in a vacuum box to remove the solvents, and the resulting dry gel was milled into powders in a mortar and then calcined in an oven at 600°C for 2 h for use. Pure TiO_2 was prepared in the same way. For convenience, the samples were labeled as TF(X), TH(Y) for Fe^{3+} and Ho^{3+} single-doped TiO_2, and TF(X)H(Y) for Fe^{3+} and Ho^{3+} codoped TiO_2, where X and Y refer to the nominal atomic concentration of Fe^{3+} and Ho^{3+}, respectively.

2.2. Characterization

XRD patterns of all samples were obtained at room temperature with a Holand X'pert PROMPD diffractometer (CuK_α radiation, $\lambda = 1.5406$ Å) operated at 45 kV and 40 mA. The crystalline size was estimated by applying the Scherrer equation $D = K\lambda/\beta\cos\theta$ to the FWHM of the (101) peak of anatase, with a-silicon (99.9999%) as a standard for the instrumental line broading. The distortion of the TiO_2 matrices was also estimated from the XRD spectra using the formula $\varepsilon = \beta/4\tan\theta$. The BET surface area was obtained by N_2 adsorption at 77 K using a micromeritics ASAP 2000. The UV-Vis absorption spectra of samples were recorded on a UV–3000 spectrophotometer in the range 300–600 nm at room temperature in air, using high pure $BaSO_4$ as the reference substance. To analyze the surface elemental composition and valent state of photocatalysts, X-ray photoelectron spectroscopy (XPS) was recorded with a VG MKII spectrometer using a radiation source of AlK_α radiation with an energy of 1486.6 eV. As an internal reference for the absolute binding energy, a C1*s* peak of 284.6 eV was used. The concentration of methyl orange in solution was measured with a spectrophotometer (DR/2500, America HACH Company).

2.3. Measurement of Photo-Catalytic Efficiency

The experiment of the photodegradation was carried out in the photo reaction system drawn in Fig. 1. Ultraviolet irradiation was offered by a 500-W high-pressure mercury lamp with major emission at 365 nm. The spectrum energy distribution of the pulsed xenon lamp known as an artificial small sun is very close to that of solar light, and its working characteristic is so stable that irradiation energy is immobile at any time. Thus, in this work, a 1500 W pulsed xenon lamp was used as the light source of simulated solar light. The reactive bottle was a 250 mL cylindrical vessel with a water-cooled quartz jacket. The lamp was located in the center of the quartz jacket. A magnetic stirrer was equipped at the bottom of the reactor to achieve effective dispersion. Air was bubbled through the reaction solution from the bottom to ensure a constant dissolved O_2 concentration.

To assess the photocatalytic activity of doped TiO_2, pure TiO_2 powder was also tested. The amount of TiO_2 powder chosen was 2 g/L. The initial methyl orange concentration was 40 mg/L for UV irradiation and 20 mg/L for simulated solar light. The temperature of the reaction solution was maintained at 30 ± 0.5°C. Some aqueous samples were withdrawn at different intervals. The residual concentration of methyl orange was measured at 465 nm with a DR/2500 spectrophotometer.

3. EXPERIMENTAL RESULTS AND DISCUSSION

3.1. X-ray Diffraction and BET-Specific Surface Area

X-ray diffraction measurements (Fig. 2) show that all samples prepared have the anatase structure. Compared to pure TiO_2, the pattern peaks for single-doped and codoped TiO_2 slightly weaken and broaden, and this phenomenon is especially obvious for Ho-doped TiO_2. A(103), A(004), and A(112) peaks of anatase for Ho-doped TiO_2 are conjoint and come to a broad diffraction peak, and the A(105) and A(211) XRD peaks tend to conjoin together, which indicates Ho doping has a strong function to restrain the increase of crystallite size. It may be ascribed to the segregation of the dopant cations at the grain boundary and prevent the growth of nanocrystallite in the nanoparticles. There is a slight broadening in XRD peaks for Fe-doped sample, and the broadened degree of peaks of TF(1)H(1) is between of them. No characteristic peak of iron and holmium oxide are found in the XRD patterns, implying either the Fe^{3+} and Ho^{3+} ions are incorporated into the crystalline part of TiO_2 or that iron and holmium oxide are very small and highly dispersed.

The radius of Ti^{4+}, Fe^{3+}, and Ho^{3+} are 0.74, 0.69, and 0.908 Å, respectively. The radius size of Ti^{4+} and Fe^{3+} was almost same; therefore, it can be inferred that the Fe ions might insert into the structure of titania and be located at interstices or occupy some of the lattice sites of TiO_2, forming an iron–titanium solid solution [24]. However, the radius of Ho^{3+} is much larger than that of Ti^{4+}. It is difficult for Ho ions to be introduced into the structure of titania, so it must be located on the grain boundary of TiO_2 and highly dispersed and, thus, prevent the growth of the crystallite size.

The particle characteristics calculated from the XRD and BET-specific surface area for the samples are summarized in the table. It can be seen that pure TiO_2 shows a low surface area and high crystallite size in comparison with the doped sample, which implies that Fe^{3+} and Ho^{3+} doping restrain the increase of crystallite size. The smaller crystalline size in the doped nanoparticles not only increased the surface areas, which is beneficial for transportation and exchanges of organic and productions, but the smaller crystallite size is also in favor of the separation of the photogenerated carriers, prolonging the lifetime of the carriers and then improving the photocatalytic activity. The unit cell volumes of doped TiO_2 particles are obvious bigger than that of undoped TiO_2 and that of codoped TiO_2 particles is the most in all samples. The matrix distortion increases in the order of TiO_2, TF(2), TF(1)H(1), and TH(2). It can be inferred that Ho doping can lead to matrix distortion and expansion, although Ho ions are difficult to introduce into the structure of titania. The recombination of photogenerated electrons and holes is the major factor to inhibit the photocatalytic activity of TiO_2. Expansion in crystal matrices can create oxygen vacancies, which generate shallow energy states below the bottom of the conduction band and served as electron trap sites in nanocrystalline TiO_2. The separation of the charge carriers is attributed to such trapping. Wang et al. [25] reported that the IPCEs (the incident

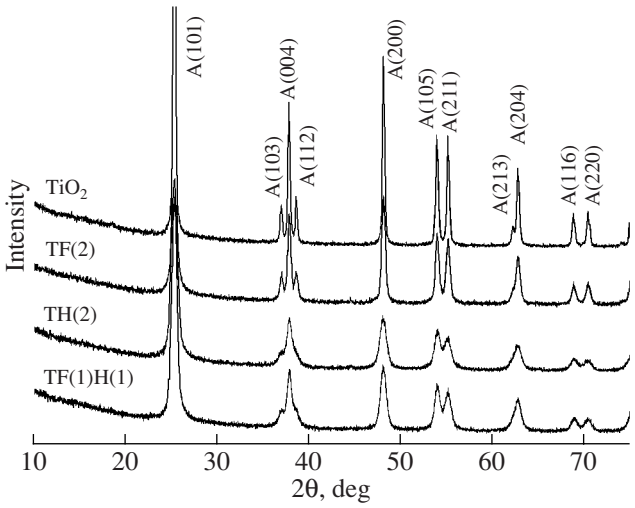

Fig. 2. XRD patterns of samples.

XRD analysis result of samples

Doped element	Doped content, %	Crystal size, nm	BET surface area, m^2/g	Matrix distortion, %	Crystal parameter		
					a, nm	*c*, nm	*V*, nm^3
None	0	51.9	38.42	0.3012	0.3888	0.8166	0.1234
Fe	2	25.5	–	0.6145	0.3885	0.8259	0.1247
Ho	2	13.0	98.81	1.1988	0.3885	0.8252	0.1245
Fe + Ho	1 + 1	13.5	78.49	1.1631	0.3884	0.8486	0.1280

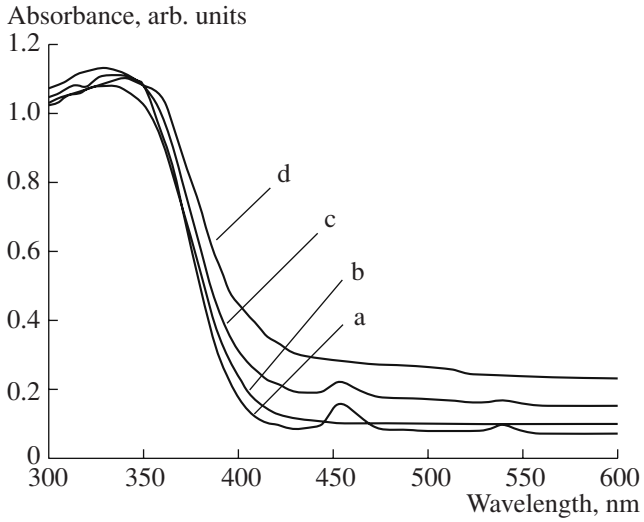

Fig. 3. UV-Vis absorption spectra of samples: (a) TH(0.5); (b) TiO_2; (c) TF(0.05)H(0.5); (d) TF(0.5).

monochromatic photon to current conversion efficiency) of Eu^{3+}-, La^{3+}-, Nd^{3+}-, and Pr^{3+}-doped TiO_2 electrodes were much larger than those of undoped TiO_2, which indicates that the photogenerated electron-hole pairs were separated more efficiently in rare-earth-doped TiO_2 nanoparticles than in pure TiO_2. So Ho doping may retard the recombination of photogenerated electrons and holes and help to improve the photocatalytic activity of TiO_2.

3.2. UV-Vis Absorption Spectra

Figure 3 shows the UV-Vis absorption spectra of Fe^{3+}-doped, Ho^{3+}-doped, codoped, and undoped TiO_2, respectively. Compared with the spectrum of pure TiO_2, a tiny blue-shift of the absorption profile in the Ho^{3+}-doped TiO_2, and a red-shift in the Fe^{3+}-doped TiO_2 are clearly observed. The sample of TF(0.05)H(0.5) shows the same red-shift, and the shifted degree is between them.

During the photocatalytic process, the absorption of photons by the photocatalyst leads to the excitation of electrons from the valence band to the conduction band, thus generating electron-hole pairs. The electron in the conduction band is captured by oxygen molecules dissolved in the suspension, and the hole in the valence band can be captured by OH^- or H_2O species adsorbed on the surface of the catalysts to produce the hydroxyl radical. Thus, the catalysis activity is strongly related to the number of electron-hole pairs in TiO_2. The more electron-hole pairs that form on the TiO_2 surface, the more highly efficient the catalysis activity in depigmentation [26]. The number of electron-hole pairs depends on the optical properties of samples. The longer the wavelength light that can be absorbed, under the same light irradiation, the more electron-hole pairs that are formed on the TiO_2 surface. From Fig. 3, it can be seen that Fe^{3+} doping leads to a red-shift of the absorption profile, which is advantageous for generating electrons and holes under photoirradiation.

3.3. X-ray Photoelectron Spectroscopy

In order to detect the peaks of dopants by XPS, a TF(5)H(5) sample with higher Fe and Ho concentrations was prepared. XPS spectra of TF(5)H(5) and pure TiO_2 are shown in Fig. 4. Peaks at around 284.6 eV are found in all survey spectra, corresponding to carbon impurities, probably arising from the background or the residual precursors. The Ti $2p_{1/2}$ and Ti $2p_{3/2}$ binding energies for undoped TiO_2 are 464.4 and 458.7 eV, respectively, and the space between them is 5.7 eV (Fig. 4b), which is in excellent agreement with the literature data for pure TiO_2 [27]. In fact, the presence of titanium with an oxidation state lower than +4 should have been evidenced by the presence of shoulders on the binding energy side of the peak, which was not observed.

The binding energies of Ti $2p_{1/2}$ and Ti $2p_{3/2}$ peaks in the TF(5)H(5) sample are 464.55 and 458.75 eV (space 5.8 eV) (Fig. 4d), which are actually the same as those in Fig. 4b within the accuracy of the XPS measurements. No Ti^{3+} species were observed by XPS. The absence of broadening of the Ti $2p_{3/2}$ signals, (FWHM = 1.4 eV for all samples) may also indicate the presence of only Ti^{4+} species [28]. Figure 4c shows the result of the O 1*s* fit spectra of TF(5)H(5). The highly asymmetric shapes with a wider left side of the oxygen XPS lines suggest different oxygen environments. The peak at 530.1 eV [29] is due to the O^{2-} ion in the TiO_2 lattice, and the peak at 531.9 eV [30] should be attributed to the surface hydroxyl groups or chemisorbed water molecules on the titania. The atomic ratio O to Ti of pure TiO_2 and TF(5)H(5) is 2.278 and 2.718, respectively, which indicates that TF(5)H(5) contains more surface hydroxyl groups or chemisorbed water molecules, which is helpful to improve the photocatalytic activity of TiO_2.

3.4. Photocatalytic Activity

The photocatalytic activity of the samples is measured by the degradation of the aqueous solution of methyl orange without concerning the degradation intermediates in detail. Before irradiating with a light, the samples are stirred in the dark for half an hour. Detection results show that the methyl orange concentration has a negligible decrease caused by slight absorption on the photocatalysts surface, which indicates that there is no degradation in the absence of irradiation.

The evolutions of methyl orange photodegradation with time under UV and simulated solar light irradiation are presented in Fig. 5. In comparison with pure TiO_2, doping improves the photocatalytic activity of TiO_2. The codoping of Fe^{3+} and Ho^{3+} can markedly

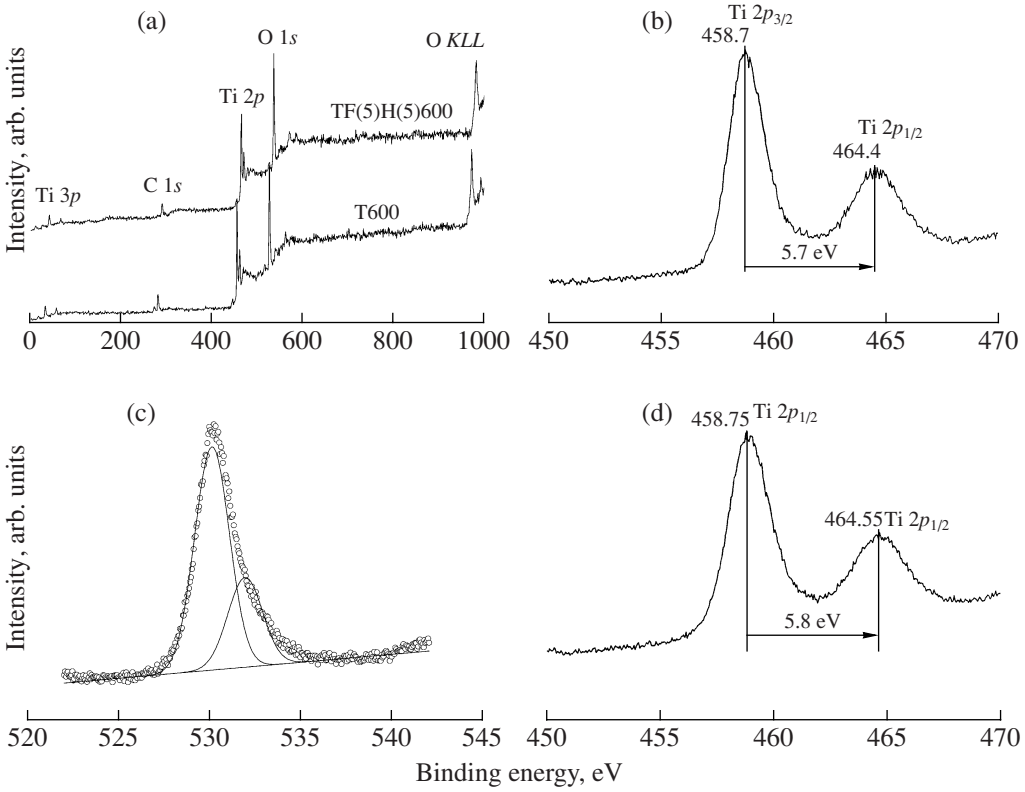

Fig. 4. XPS spectra of pure TiO_2 and TF(5)H(5): (a) survey; (b) Ti 2*p* peaks in undoped TiO_2; (c) O 1*s* peaks; (d) Ti 2*p* peaks in TF(5)H(5).

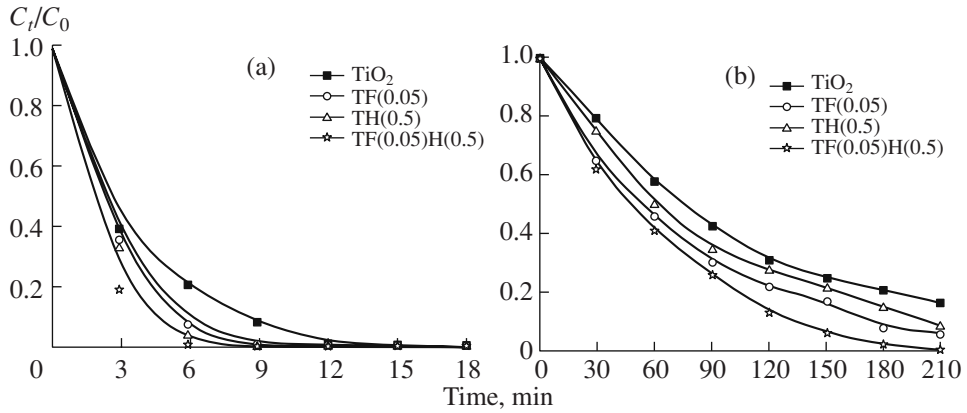

Fig. 5. Degradation curves of methyl orange with irradiation time: (a) UV light; (b) simulant solar light.

enhance the photocatalytic activity relative to undoped and single-doped TiO_2. Such an improvement implies that there is a synergistic effect in catalytic activity when both Fe^{3+} and Ho^{3+} are codoped into the nanocrystalline TiO_2 particles.

From Fig. 5a, it can be seen that the degradation efficiency of the Ho^{3+}-doped sample under UV irradiation is higher than that of Fe^{3+}-doped sample; the reason for this may be that the inhibition function of recombination of photogenerated electrons and holes plays a dominant role in this condition. When the irradiation light changes from UV to solar light, the red-shift of the absorption profile plays a dominant role, so the degradation efficiency of the Ho^{3+}-doped sample under simulated solar light irradiation is lower than that of the Fe^{3+}-doped sample (as was shown in Fig. 5b). When both Fe^{3+} and Ho^{3+} are codoped into the nanocrystalline TiO_2 particles, a cooperative operation will be produced. Fe^{3+}-doping broadens the absorption profile, improves photo utilization of TiO_2, and then generates

more electron-hole pairs. Ho^{3+}-doping restrains the increase in the grain size, leads to crystal expansion and matrix distortion, and retards the recombination of the photoexcited charge carriers. Thus, the photocatalytic activity of TiO_2 codoped with Fe^{3+} and Ho^{3+} is markedly improved.

4. CONCLUSIONS

Single-doped and codoped TiO_2 nanoparticles were prepared successfully by the sol-gel method. It has been found that the addition of Ho^{3+} to the TiO_2 system leads to crystal expansion and distortion of matrices, which suppress the recombination of excited electrons and holes and help to improve the photocatalytic activity of TiO_2. And Ho^{3+} doping restrains the increase of crystalline size, which is in favor of the separation of the photogenerated carriers, prolongs the lifetime of the carriers, and then improves the photocatalytic activity of TiO_2. Furthermore, the addition of Fe^{3+} to the TiO_2 system leads to a red-shift of the absorption profile of TiO_2 and improves photo utilization of TiO_2, which is advantaged to generating electrons and holes under photoirradiation. When both Fe^{3+} and Ho^{3+} are codoped into the nanocrystalline TiO_2 particles, a cooperative operation will be produced. Fe^{3+}-doping broadens the absorption profile, improves photo utilization of TiO_2, and then generates more electron-hole pairs. Ho^{3+}-doping restrains the increase of the grain size, leads to crystal expansion and matrix distortion, and retards the recombination of the photoexcited charge carriers. The photocatalytic activity of TiO_2 codoped with Fe^{3+} and Ho^{3+} ions is markedly improved related to the cooperative actions of the two dopants. It can be expected that the photocatalytic activity can be further improved by choosing proper dopants.

ACKNOWLEDGMENTS

This research was supported in part by the Corporation of Shtar Science and Technology.

REFERENCES

1. Lachheb, H., Puzenat, E., Houas, A., Ksibi, M., Elaloui, E., Guillard, C., and Herrmann J.M., *Appl. Catal., B*, 2002, vol. 39, p. 75.
2. Zielinska, B., Grzechulska, J., and Morawski, A.W., *J. Photochem. Photobiol., A*, 2003, vol. 157, p. 65.
3. Vionea, D., Minero, C., Maurinoa, V., Carlotti, M.E., Picatonotto, T., and Pelizzetti, E., *Appl. Catal., B*, 2005, vol. 58, p. 79.
4. Bessekhouad, Y., Robert, D., and Weber, J.V., *J. Photochem. Photobiol., A*, 2004, vol. 163, p. 569.
5. Wang, R., Xin, J.H., Yang, Y., Liu, H., Xu, L., and Hu, J., *Appl. Surf. Sci.*, 2004, vol. 227, p. 312.
6. Sakthivel, S., Neppolian, B., Shankar, M.V., Arabindoo, B., Palanichamy, M., and Murugesan, V., *Sol. Energy Mater. Sol. Cells*, 2003, vol. 11, p. 65.
7. Topalov, A.S., Sojic, D.V., Molnar-Gabor, D.A., Abramovic, B.F., and Comor, M.I., *Appl. Catal., B*, 2004, vol. 54, p. 125.
8. Zhang, L., Kanki, T., Sano, N., and Toyoda, A., *Sep. Purif. Technol.*, 2003, vol. 31, p. 105.
9. Wu, J.C.S. and Chen, C.H., *J. Photochem. Photobiol., A*, 2004, vol. 163, p. 509.
10. Yang, Y., Li, X., Chen, J., and Wang, L., *J. Photochem. Photobiol., A*, 2004, vol. 163, p. 517.
11. Wang, C., Bottcher, C., Bahnemann, D.W., and Dohrmann, J.K., *J. Nanopart. Res.*, 2004, vol. 6, p. 119.
12. Sun, B., Reddy, E.P., and Smirniotis, P.G., *Appl. Catal., B*, 2005, vol. 57, p. 139.
13. Zhang, W., Li, Y., Zhu, S., and Wang, F., *Catal. Today*, 2004, vols. 93–95, p. 589.
14. Xu, J., Lu, M., Guo, X., and Li, H., *J. Mol. Catal. A: Chem.*, 2005, vol. 226, p. 123.
15. Xie, Y. and Yuan, C., *Mater. Res. Bull.*, 2004, vol. 39, p. 533.
16. Xie, Y. and Yuan, C., *Appl. Catal., B*, 2003, vol. 46, p. 251.
17. Baiju, K.V., Sibu, C.P., Rajesh, K., Krishna, PillaiP., Mukundan, P., Warrier, K.G.K., and Wunderlich, W., *Mater. Chem. Phys.*, 2005, vol. 90, p. 123.
18. Xu, A.W., Gao, Y., and Liu, H.Q., *J. Catal.*, 2002, vol. 207, p. 151.
19. Chen, S.Y., Ting, C.C., and Hsieh, W.F., *Thin Solid Films*, 2003, vol. 434, p. 171.
20. Wei, H., Wu, Y., Lun, N., and Zhao, F., *J. Mater. Sci.*, 2004, vol. 39, p. 1305.
21. Yang, P., Mengkai, XuD., Yuan, D., Song, C., Liu, S., and Cheng, X., *Opt. Mater.*, 2003, vol. 24, p. 497.
22. Wang, J., Yin, S., Komatsu, M., and Sato, T., *J. Eur. Ceram. Soc.*, 2005, vol. 25, p. 3207.
23. Zhang, Z., Wang, C., Zakaria, R., and Ying, J.Y., *J. Phys. Chem. B*, 1998, vol. 102, p. 10 871.
24. Wang, C.Y., Bottcher, C., Bahnemann, D.W., and Dohrmann, J.K., *J. Mater. Chem.*, 2003, vol. 13, p. 2322.
25. Wang, Y.Q., Cheng, H.M., Zhang, L., Hao, Y.Z., Ma, J.M., Xu, B., and Li, W.H., *J. Mol. Catal. A: Chem.*, 2000, vol. 151, p. 205.
26. Gou, Y.Q., Chen, D.Y., and Su, Z.X., *Appl. Catal., A*, 2004, vol. 261, p. 15.
27. Liu, F.M. and Wang, T.M., *Appl. Surf. Sci.*, 2002, vol. 195, p. 284.
28. Zhang, W., Li, Y., Zhu, S., and Wang, F., *Chem. Phys. Lett.*, 2003, vol. 373, p. 333.
29. Borgmann, D., Hums, E., Hopfengartner, G., Wedler, G., Spitznagel, G.W., and Rademacher, I., *J. Electron. Spectrosc. Relat. Phenom.,* 1993, vol. 63, p. 91.
30. Atrens, A. and Lim, A.S., *Appl. Phys. A*, 1990, vol. 51, p. 411.